Symbol Detection Technique for Multiuser Systems Empowered by Reconfigurable Intelligent Surfaces

Rabah Ouchikh, Thierry Chonavel, Abdeldjalil Aissa El Bey, Mustapha Djeddou

Symbol Detection Technique for Multiuser Systems Empowered by Reconfigurable Intelligent Surfaces

Rabah Ouchikh
Lab Télécommunications
Ecole Militaire Polytechnique
Bordj El-Bahri, Algeria
ouchikh16rabah@gmail.com

Thierry Chonavel
IMT Atlantique, Lab-STICC,
UMR CNRS 6285, F-29238,
Brest, France
thierry.chonavel@imt-atlantique.fr

Abdeldjalil Aïssa-El-Bey
IMT Atlantique, Lab-STICC,
UMR CNRS 6285, F-29238,
Brest, France
abdeldjalil.aissaelbey@imt-atlantique.fr

Mustapha Djeddou
Electronics Department
National Polytechnic School
Algiers, Algeria
mustapha.djeddou@g.enp.edu.dz

***Abstract*—Reconfigurable Intelligent Surfaces (RIS) stand as a pivotal technology in the realm of next-generation wireless communications, offering programmable radio propagation environments. Comprising multiple reflecting elements, RIS enable optimization of their phase and amplitude to attain desired reflection characteristics. However, the passive reflecting nature of RIS poses substantial challenges for channel estimation, making coherent symbol detection a formidable task. In modern communication systems, meeting the escalating throughput demands entails equipping Base Stations (BS) with multiple antennas for simultaneous communication with numerous users, enhancing spectral efficiency in Multi-User Multiple-Input Multiple-Output (MU-MIMO) systems. Symbol detection emerges as a key challenge in such systems, necessitating the retrieval of multiple symbols transmitted over the uplink channel. In this paper, we investigate the uplink of RIS-aided MU-MIMO systems and propose a low-complexity algorithm for symbol detection. We derive a simple data detection model using the virtual angular domain representation and precoding for data symbols, followed by the introduction of an iterative symbol detection (ISD) algorithm based on the symbol-by-symbol Maximum A Posteriori (MAP) criteria. Our algorithm reduces computational complexity by incorporating the finite nature of the data alphabet and addressing the sparsity of the sensing matrix through the virtual angular domain representation.**

***Index Terms*—RIS, MU-MIMO, Symbol detection, Iterative algorithm.**

I. Introduction

Reconfigurable Intelligent Surfaces (RIS) have gained significant attention in the development of future wireless communication systems due to their ability to manipulate the propagation of radio waves. By adjusting the phase and amplitude of the signals they reflect, RIS can shape the wireless environment to enhance communication performance. However, their passive nature complicates the process of channel estimation, which in turn makes coherent symbol detection a particularly demanding challenge [1].

At the same time, modern wireless networks face increasing throughput demands, pushing Base Stations (BS) to incorporate advanced techniques such as Multi-User Multiple-Input Multiple-Output (MU-MIMO). By using multiple antennas to serve multiple users simultaneously, these systems can significantly improve spectral efficiency. Nonetheless, detecting the symbols sent by multiple users over the uplink channel remains a critical issue, as the BS must accurately decode the information transmitted by each user [2].

The Maximum Likelihood (ML) detector is considered optimal as it allows for the joint detection of all symbols belonging to a given alphabet. However, due to its exhaustive search over the data symbols to find the optimal solution, its complexity becomes high [3]. The Zero Forcing (ZF) and Minimum Mean Square Error (MMSE) detectors achieve significantly lower computational complexity compared to the ML detector. As a trade-off, the ZF/MMSE detectors exhibit inferior performance in terms of Bit Error Rate (BER) compared to the ML detector [4]. Alternative low-complexity symbol detection methods typically rely on separate detection or iterative interference cancellation techniques [2]. These approaches enable achieving performance close to Maximum A Posteriori (MAP) approach while maintaining complexity that scales linearly with the number of users.

In this paper, we investigate the uplink communication mode of RIS-aided MU-MIMO systems and introduce a low-complexity algorithm for symbol detection. We first derive a simple data detection model using the virtual angular domain representation and precoding for the data symbols. Then, we propose an iterative symbol detection (ISD) algorithm. The proposed algorithm is based on the symbol-by-symbol MAP criteria. To reduce computational complexity, this algorithm incorporates the finite nature of the alphabet to which the data belong and also addresses the sparsity of the sensing matrix by leveraging the virtual angular domain representation.

Notation: Let a, $\boldsymbol{a}$, and $\boldsymbol{A}$ denote a scalar, a column vector, and a matrix, respectively. $\mathbb{E}\{.\}$ represents the expectation operation. The notation $diag\{d_1, d_2, ..., d_N\}$ denotes the $N \times N$ diagonal matrix with entry (i, i) equal to d_i. Transposition and Hermitian transposition are denoted respectively by the superscripts $(.)^T$ and $(.)^H$. $\boldsymbol{I}_N$ represent the $N \times N$ identity matrix. $\mathcal{CN}(m, \sigma^2)$ is the complex Gaussian distribution with mean m and variance σ^2.

II. System model

The considered RIS-aided MU-MIMO uplink system is illustrated in Fig. 1. In this scene, a total of K user terminals (UTs), each equipped with N_k antennas, simultaneously transmit data symbols to a multi-antenna base station (BS).

The UTs are indexed by the set $\mathcal{K} = \{1, 2, ..., K\}$. The communication between the UTs and the BS is facilitated by an RIS comprising N programmable reflecting elements, denoted by the set $\mathcal{N} = \{1, 2, ..., N\}$. These reflecting elements are dynamically controlled by a smart controller to adjust their reflection properties in real-time [5]. Direct transmissions from UTs to the BS are assumed blocked due to unfavorable propagation conditions, such as significant obstacles, and are thus disregarded in the system model. This assumption is commonly made in the literature [6]. Furthermore, only the reflections occurring once are considered, while subsequent reflections with negligible power are ignored due to factors like high path loss.

The matrix representing the channel from the RIS to the BS is denoted as $\boldsymbol{H}_1 \in \mathbb{C}^{M \times N}$, where M represents the number of antennas at the BS. The Saleh-Valenzuela channel model is commonly employed to characterize $\boldsymbol{H}_1$, and it is represented as [7]

$$\boldsymbol{H}_1 = \sqrt{\frac{MN}{L_1}} \sum_{i=1}^{L_1} \alpha_i^{H_1} \boldsymbol{b}\left(\theta_i^{H_r}, \xi_i^{H_r}\right) \boldsymbol{a}\left(\theta_i^{H_t}, \xi_i^{H_t}\right)^T, \quad (1)$$

where L_1 denotes the total number of paths between the RIS and the BS. The parameters $\alpha_i^{H_1}$, $\theta_i^{H_r}$ ($\xi_i^{H_r}$), and $\theta_i^{H_t}$ ($\xi_i^{H_t}$) correspond to the complex gain consisting of path loss and azimuth (elevation) angles at the BS and RIS, respectively, for the i-th path. Additionally, the channel from UT k to the RIS is represented by $\boldsymbol{H}_{2,k} = [\boldsymbol{h}_{2,1}, \boldsymbol{h}_{2,2}, ..., \boldsymbol{h}_{2,N_k}] \in \mathbb{C}^{N \times N_k}$ for all k. Using the Saleh-Valenzuela channel model, $\boldsymbol{h}_{2,k}$ can be represented by

$$\boldsymbol{h}_{2,k} = \sqrt{\frac{N}{L_{2,k}}} \sum_{j=1}^{L_{2,k}} \alpha_j^{2,k} \boldsymbol{a}\left(\theta_j^{2,k}, \xi_j^{2,k}\right), \quad (2)$$

where $L_{2,k}$ denotes the total number of paths between the k-th UT and the RIS. The parameters $\alpha_j^{2,k}$, $\theta_j^{2,k}$ ($\xi_j^{2,k}$) represent the complex gain, which consists of path loss and azimuth (elevation) angle at the RIS, for the j-th path associated with UT k. Furthermore, $\boldsymbol{b}(\theta, \xi) \in \mathbb{C}^{M \times 1}$ and $\boldsymbol{a}(\theta, \xi) \in \mathbb{C}^{N \times 1}$ represent the normalized array steering vector associated with the BS and the RIS, respectively. For a typical $N_1 \times N_2$ ($N = N_1 \times N_2$) Uniform Planar Array (UPA), $\boldsymbol{a}(\theta, \xi)$ can be expressed as [7]

$$\boldsymbol{a}(\theta, \xi) = \frac{1}{\sqrt{N}} [e^{-j2\pi d \sin(\theta)\cos(\xi)\boldsymbol{n}_1/\lambda}] \otimes [e^{-j2\pi d \sin(\xi)\boldsymbol{n}_2/\lambda}], \quad (3)$$

where $\boldsymbol{n}_i = [0, 1, ..., N_i - 1]^T$ $(i = 1, 2)$ represent the indices for the antenna elements along the first and second dimensions of the UPA. λ denotes the carrier wavelength, and d represents the antenna spacing, typically satisfying $d = \lambda/2$.

We represent $\boldsymbol{x}_k \in \mathbb{C}^{N_k \times 1}$ as the transmitted signal by UT k with zero-mean and covariance matrix $\boldsymbol{C}_k = \mathbb{E}\{\boldsymbol{x}_k \boldsymbol{x}_k^H\}$. Additionally, we highlight that $\boldsymbol{x}_k$ is independent of the signals transmitted by other UTs, i.e., $\mathbb{E}\{\boldsymbol{x}_k \boldsymbol{x}_l^H\} = \boldsymbol{0}$ $\forall k \neq l$ and the entries of $\boldsymbol{x}_k$ belong to a finite alphabet such as QAM or PSK. The received signal at the BS can be expressed as:

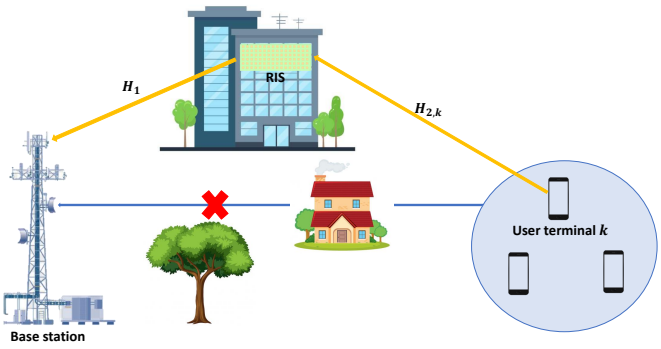

Fig. 1: The considered RIS-aided MU-MIMO uplink system.

$$\boldsymbol{y} = \sum_{k=1}^{K} \boldsymbol{H}_1 \boldsymbol{\Phi} \boldsymbol{H}_{2,k} \boldsymbol{x}_k + \boldsymbol{n}, \quad (4)$$

where $\boldsymbol{n} \in \mathbb{C}^{M \times 1}$ is the received noise at the BS and $\boldsymbol{\Phi} = diag\{\phi_1, \phi_2, ..., \phi_N\}$ denotes the RIS phase shift matrix.

III. Proposed Symbol Detection Approach

In this section, we present the proposed algorithm allowing the detection of the vectors $\boldsymbol{x}_k$ containing the data symbols of the K users based on the model (4).

A. Proposed model

By adopting the widely used orthogonal data transmission strategy among users, the uplink symbol detection associated with different users can be independent. Therefore, the received signal $\boldsymbol{y}_k \in \mathbb{C}^{M \times 1}$ at the BS for the contribution of the k-th UT can be expressed as:

$$\boldsymbol{y}_k = \boldsymbol{H}_1 \boldsymbol{\Phi} \boldsymbol{H}_{2,k} \boldsymbol{x}_k + \boldsymbol{n}_k, \ \forall k \in \mathcal{K}. \quad (5)$$

where $\boldsymbol{n}_k \sim \mathcal{CN}(\boldsymbol{0}, \sigma^2 \boldsymbol{I}_M)$ represents the additive white Gaussian noise. We denote $\boldsymbol{G}_k = \boldsymbol{H}_1 \boldsymbol{\Phi} \boldsymbol{H}_{2,k}$ as the cascaded channel weighted by the RIS matrix $\boldsymbol{\Phi}$. By using the virtual angular domain representation [7], $\boldsymbol{G}_k$ can be decomposed as

$$\boldsymbol{G}_k = \boldsymbol{U}_M \tilde{\boldsymbol{G}}_k \boldsymbol{U}_N^T, \quad (6)$$

where $\tilde{\boldsymbol{G}}_k$ denotes the $M \times N$ angular cascaded channel weighted by the RIS matrix, $\boldsymbol{U}_M$ and $\boldsymbol{U}_N$ are respectively the $M \times M$ and $N \times N$ dictionary unitary matrices at the BS and the RIS. Given the limited scattering around the BS and the RIS, $\tilde{\boldsymbol{G}}_k$ has only a few non-zero elements, demonstrating sparsity.

By substituting (6) into (5), we obtain

$$\boldsymbol{y}_k = \boldsymbol{U}_M \tilde{\boldsymbol{G}}_k \boldsymbol{U}_N^T \boldsymbol{x}_k + \boldsymbol{n}_k. \quad (7)$$

Letting $\tilde{\boldsymbol{y}}_k = \boldsymbol{U}_M^H \boldsymbol{y}_k$ and by employing precoding for the data symbols prior to transmission (This precoding involves transmitting $(\boldsymbol{U}_N^T)^H \boldsymbol{x}_k$ instead of $\boldsymbol{x}_k$), equation (7) becomes

$$\tilde{\boldsymbol{y}}_k = \tilde{\boldsymbol{G}}_k \boldsymbol{x}_k + \boldsymbol{n}_k. \tag{8}$$

Based on (8), the proposed algorithm enables the detection of the data symbols vector $\boldsymbol{x}_k$ for each UT k. This algorithm takes into consideration the finite alphabet of the entries of $\boldsymbol{x}_k$ and leverages the sparsity of $\tilde{\boldsymbol{G}}_k$ to mitigate computational complexity.

B. Proposed algorithm

Due to the sparsity of $\tilde{\boldsymbol{G}}_k$, the system is represented as a sparsely connected factor graph, comprising N variable nodes and M observation nodes corresponding to $\boldsymbol{x}_k$ and $\boldsymbol{y}_k$ respectively. Exploiting $\tilde{\boldsymbol{G}}_k$'s sparsity, each variable node $\boldsymbol{x}_k(c)$ is connected only to N_i^c observation nodes $\{\boldsymbol{y}_k(l_i), l_i \in \mathcal{I}_c\}$, and each observation node $\boldsymbol{y}_k(r)$ is connected solely to N_i^r variable nodes $\{\boldsymbol{x}_k(l_i), l_i \in \mathcal{I}_r\}$, where $\mathcal{I}_c$ and $\mathcal{I}_r$ represent the sets of non-zero indices in the c-th column and the r-th row of $\tilde{\boldsymbol{G}}_k$, respectively. Applying the MAP criterion to Eq. (8) results in:

$$\hat{\boldsymbol{x}}_k = \underset{\boldsymbol{x}_k \in \mathcal{A}^N}{\arg\max}\ Pr(\boldsymbol{x}_k | \boldsymbol{y}_k, \tilde{\boldsymbol{G}}_k), \tag{9}$$

where $\mathcal{A}$ represents the alphabet to which the entries $\boldsymbol{x}_k$ belong. Equation (9) exhibits an NP-hard problem. Utilizing Bayes theorem and assuming independence among the elements of $\boldsymbol{y}_k$ for a given $\boldsymbol{x}_k(i)$, $i = 1 : N$ (this assumption is justified by the sparsity of $\tilde{\boldsymbol{G}}_k$). The application of the MAP criterion symbol-by-symbol to (9) yields

$$\hat{\boldsymbol{x}}_k(r) = \underset{m_j \in \mathcal{A}}{\arg\max} \prod_{l \in \mathcal{I}_r} Pr(\boldsymbol{y}_k(l) | \boldsymbol{x}_k(r) = m_j, \tilde{\boldsymbol{G}}_k), \tag{10}$$

for $l = 0 : M-1$ and $r = 0 : N-1$. The proposed algorithm unfolds as follows: Firstly, the symbol probabilities will be initialized as follows:

$$Pr_{c,r}^{(0)}(\boldsymbol{x}_k(r)) = \frac{1}{|\mathcal{A}|},\ \forall r \in \{0, 1, ..., .N-1\}. \tag{11}$$

Subsequently, the association between the element $\boldsymbol{y}_k(r)$ of the observation vector and the element $\boldsymbol{x}_k(c)$ will be defined as follows:

$$\boldsymbol{y}_k(r) = \tilde{\boldsymbol{G}}_k(r, c)\boldsymbol{x}_k(c) + e_{rc}, \tag{12}$$

where $\tilde{\boldsymbol{G}}_k(r, c)$ denotes the (r, c)-th element of $\tilde{\boldsymbol{G}}_k$ and e_{rc} is the interference-plus-noise, which is given by

$$e_{rc} = \boldsymbol{x}_k(\mathcal{I}_r)^T \tilde{\boldsymbol{G}}_k(r, \mathcal{I}_r) + \boldsymbol{n}(r), \tag{13}$$

where $\boldsymbol{x}_k(\mathcal{I}_r)$ is a vector formed by the entries of $\boldsymbol{x}_k$ at indices $\mathcal{I}_r$ and $\tilde{\boldsymbol{G}}_k(r, \mathcal{I}_r)$ is a vector formed by the non-zero elements of the r-th row of $\tilde{\boldsymbol{G}}_k$. $e_{rc} \sim \mathcal{CN}(m_{r,c}, \sigma_{r,c}^2)$.

Then, the observation node $\boldsymbol{y}_k(r)$ conveys to the variable node $\boldsymbol{x}_k(c)$ the mean and variance of the interference term. These two parameters are computed using the following formulas:

$$m_{r,c} = \sum_{k \in \mathcal{J}_r, k \neq c} \sum_{i=1}^{\mathcal{A}} m_i Pr_{r,k}(m_i) \tilde{\boldsymbol{G}}_k(r, k), \tag{14}$$

$$\sigma_{r,c}^2 = \sum_{k \in \mathcal{J}_r, k \neq c} \sum_{i=1}^{\mathcal{A}} |m_i|^2 Pr_{r,k}(m_i) |\tilde{\boldsymbol{G}}_k(r, k)|^2 + \xi_{r,c}. \tag{15}$$

where $\xi_{r,c} = \sigma^2 - |m_{r,c}|^2$. Consequently, $\boldsymbol{x}_k(c)$ utilizes these two parameters to compute the elements of the probability mass function (PMF) vector $\boldsymbol{Pr}_{r,c}$. Once computed, these elements, as expressed by the formula below, are transmitted to $\boldsymbol{y}_k(r)$.

$$Pr_{c,r} \propto -\exp\left(\sum_{l \in \mathcal{J}_c, l \neq c} \frac{|\boldsymbol{y}_k(l) + m_{l,c} + \tilde{\boldsymbol{G}}_k(l, c) m_i|}{\sigma_{r,c}^2} \right). \tag{16}$$

This message passing process between $\boldsymbol{y}_k(r)$ and $\boldsymbol{x}_k(c)$ will persist until convergence at iteration t, as indicated by the following condition:

$$|Pr_{c,r}^{(t)} - Pr_{c,r}^{(t-1)}| < \epsilon,$$

for all (r, c) pairs, where ϵ is a suitable small value.

Finally, the symbols $\boldsymbol{x}_k(c)$, for $c = 0 : N-1$ are estimated based on $Pr_{c,r}^{(t)}(m_i)$ as follows:

$$\hat{\boldsymbol{x}}_k(c) = \underset{m_i \in \mathcal{A}}{\arg\max}\ Pr_{c,r}^{(t)}(m_i),\ c = 0 : N-1. \tag{17}$$

The steps of the algorithm are summarized in Algorithm 1.

Algorithm 1 Iterative symbol detection (ISD) algorithm.

Input: $\boldsymbol{y}_k \in \mathbb{C}^{M \times 1}$, $\tilde{\boldsymbol{G}}_k \in \mathbb{C}^{M \times N}$, $\mathcal{A}$, σ^2, ϵ

Initialization: $\mathbf{Pr}_{c,r}^{(0)} = \frac{1}{|\mathcal{A}|}$, $\forall r \in \{0, 1, ..., .N-1\}$ and $c \in \mathcal{I}_r$, Counter $t = 1$,

repeat

Pass the mean $m_{r,c}^{(t)}$ in (14) and variance $(\sigma_{r,c}^2)^{(t)}$ in (15) from observation nodes $\boldsymbol{y}_k$ to variable nodes $\boldsymbol{x}_k(c)$ for $c \in \mathcal{I}_r$,

At $\boldsymbol{x}_k(c)$, update the PMF as follows: $Pr_{c,r}^{(t)}(m_j) = \Delta Pr_{c,r}^{(t)}(m_j) + (1-\Delta) Pr_{c,r}^{(t-1)}(m_j)$, then transmit it to the observation nodes $\boldsymbol{y}_k(r)$ for $r \in \mathcal{I}_c$,

Update the decision on the transmitted symbols $\boldsymbol{x}_k$ using (17), and obtain $\hat{\boldsymbol{x}}_k$,

$t = t + 1$,

until $|Pr_{c,r}^{(t)} - Pr_{c,r}^{(t-1)}| < \epsilon$,

Output: $\hat{\boldsymbol{x}}_k$.

C. Computational complexity

In this section, we derive the computational complexity of the proposed algorithm and compare it to the ZF, MMSE, and ML detectors.

TABLE I: Computational complexities of ZF, MMSE, ML and the proposed detector.

Detector	Computational complexity
ZF/MMSE	$\mathcal{O}(KN^3)$
ML	$\mathcal{O}(K\|\mathcal{A}\|^N)$
Proposed ISD algorithm	$\mathcal{O}(n_{iter}K(M+N)P\|\mathcal{A}\|)$

The complexity of one iteration of the detection algorithm involves computing (14), (15), (16), and (17). Each of (14) and (15) has a complexity of $\mathcal{O}(KMP|\mathcal{A}|)$. Furthermore, the complexities of (16) and (17) are $\mathcal{O}(KNP|\mathcal{A}|)$ and $\mathcal{O}(KN|\mathcal{A}|)$. Therefore, the overall complexity of the data detection algorithm is dominated by $\mathcal{O}(n_{iter}K(M+N)P|\mathcal{A}|)$, where n_{iter} is the number of iterations required for the convergence of the data detection algorithm and P represents the average number of non-zero elements in each row and each column of $\tilde{\boldsymbol{G}}_k$.

Table I provides a comparison in terms of computational complexity between the proposed algorithm and the ZF, MMSE, and ML detectors.

The proposed algorithm requires about twenty iterations to converge ($n_{iter} \sim 20$). From Table I, it is shown that the complexity of all three algorithms varies linearly with the number of users K. However, only the complexity of the ISD algorithm varies linearly with both the number of antennas at the base station M and the number of elements in the RIS N. This is in contrast to the ZF and MMSE detectors, where the complexity varies with N^3, and the ML detector, where it varies with $|\mathcal{A}|^N$. Therefore, the proposed algorithm is less complex when compared to the ZF, MMSE, and ML detectors.

IV. Simulation Results

In this simulation, we investigate a scenario characterized by specific parameters: a system comprising $M = 256$ BS antennas ($M_1 = 16$, $M_2 = 16$), interacts with an environment featuring $N = 256$ RIS elements ($N_1 = 16$, $N_2 = 16$). Serving $K = 16$ users, the system encounters multi-path propagation, with $L_1 = 50$ paths between the RIS and the BS, and $L_2 = 100$ paths from each user to the RIS. Spatial angles are on the quantization intervals. The RIS operates with discrete phase shifts, with each reflecting element capable of selecting from the set $\{-\frac{1}{\sqrt{N}}, \frac{1}{\sqrt{N}}\}$. Channel attenuation between the BS and RIS is given as $|\alpha_i^{H_1}| = 10^{-3}d_1^{-2.2}$, where $d_1 = 10$ meters is the distance between the BS and the RIS. Similarly, the attenuation between the RIS and users is given by $|\alpha_j^{2,k}| = 10^{-3}d_2^{-2.8}$, where $d_2 = 100$ meters is the distance between the RIS and user k $\forall k$ [7]. For symbol modulation, we choose Binary Phase Shift Keying (BPSK).

We compare the proposed ISD algorithm to the ZF, MMSE, and ML detectors.

Figure 2 shows the evolution of BER as a function of SNR for the proposed ISD algorithm. The main objective of this simulation is to demonstrate the performance gain achieved by using the RIS compared to a system without RIS. As illustrated by the curve, the integration of RIS significantly reduces the BER over a given SNR range, indicating better data detection efficiency and a noticeable improvement in the system's robustness against time-varying channels. This enhanced performance is attributed to RIS's ability to dynamically adjust the communication channel in real-time, thereby optimizing the link between the transmitter and the receiver.

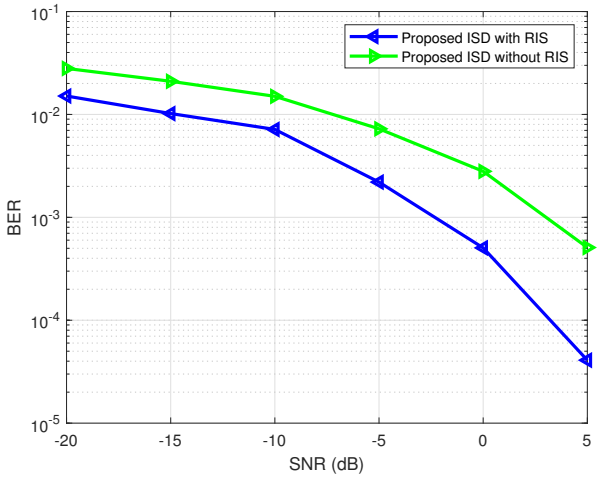

Fig. 2: BER versus SNR for the ISD algorithm with and without RIS assistance.

Figure 3 illustrates the BER as a function of the number of iterations required for the convergence of the proposed ISD algorithm for three different SNR values (-5, 0 and 5 dB). The purpose of this figure is to show how the BER evolves during the iterative process and to demonstrate the algorithm's convergence behavior. For all three SNR values, the algorithm successfully converges after approximately twenty iterations. This indicates that the proposed algorithm maintains stable and efficient performance across different SNR levels, requiring a relatively small number of iterations to reach convergence and ensuring a rapid reduction in BER as the iterations progress.

Figure 4 depicts a comparison in terms of BER between the proposed algorithm and the ZF, MMSE, and ML detectors. As shown in Figure 4, MMSE outperforms ZF at low SNR values, and these two estimators tend to converge towards the same values of BER as SNR increases. This is supported by the fact that the multiplication term between the noise and the inverse of the detection matrix might amplify the latter due to the high power of the noise. However, at high SNR, this term becomes increasingly negligible, resulting in the performance of ZF approaching that of MMSE. It is also shown from Figure 4 that the proposed algorithm outperforms both ZF and MMSE (by approximately 7 dB at BER $= 10^{-3}$). However, it is less efficient than ML. This is because ML is the optimal detector but the most complex one. Therefore, the suggested algorithm achieves a good compromise between BER performance and complexity.

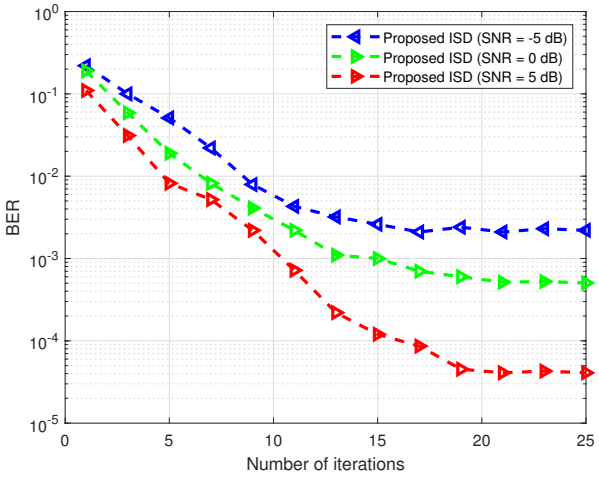

Fig. 3: BER versus number of iterations for the convergence of the proposed algorithm for three SNR values ($M = N = 256$, $K = 16$, $|\mathcal{A}| = 2$).

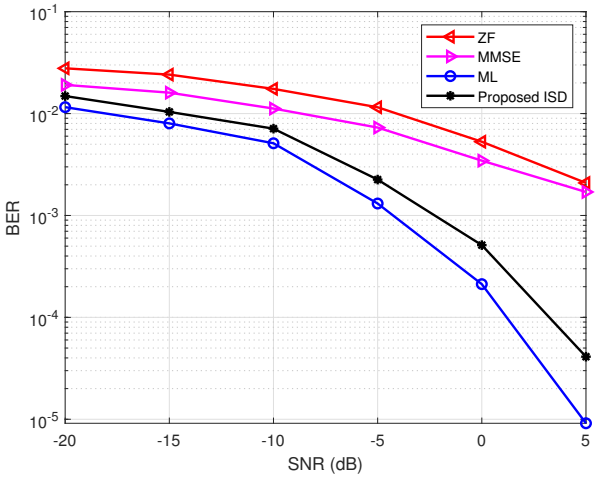

Fig. 4: BER performance of the proposed and ZF, MMSE and ML detectors ($M = N = 256$, $K = 16$, $|\mathcal{A}| = 2$).

V. Conclusion

In this article, we have addressed the challenging problem of symbol detection in RIS-assisted MU-MIMO systems. We have proposed a low-complexity iterative symbol detection algorithm, based on MAP criterion. Virtual angular domain representation and precoding are used to facilitate the modelling of the symbol detection problem. The proposed approach provides an efficient solution to address the challenge of computational complexity while maintaining robust symbol detection performance in RIS-enabled wireless networks. The results from simulations highlight the advantages of the proposed algorithm both in terms of performance and complexity compared to conventional detectors. For future research, it would be beneficial to use this algorithm with a channel estimation method to jointly estimate the channel and detect data symbols.

References

[1] A. K. Shrivastava, U. K. Agrawal, M. K. Shukla, and O. J. Pandey, "Neural networks based phase estimation and symbol detection for RIS-assisted wireless communications," *IEEE Communications Letters*, 2023.

[2] L. Wang, N. Shlezinger, G. C. Alexandropoulos, H. Zhang, B. Wang, and Y. C. Eldar, "Jointly learned symbol detection and signal reflection in RIS-aided multi-user MIMO systems," in *55th Asilomar Conference on Signals, Systems, and Computers*. IEEE, 2021, pp. 715–721.

[3] Q. Li, M. Wen, Y. Huang, J. Wen, J. Li, and E. Basar, "Reconfigurable intelligent surface-aided single-carrier frequency-domain equalization," in *GLOBECOM IEEE Global Communications Conference*. IEEE, 2023, pp. 2505–2510.

[4] Q. Li, M. Wen, E. Basar, G. C. Alexandropoulos, K. J. Kim, and H. V. Poor, "Channel estimation and multipath diversity reception for RIS-empowered broadband wireless systems based on cyclic-prefixed single-carrier transmission," *IEEE Transactions on Wireless Communications*, 2023.

[5] C. You, B. Zheng, and R. Zhang, "Channel estimation and passive beamforming for intelligent reflecting surface: Discrete phase shift and progressive refinement," *IEEE Journal on Selected Areas in Communications*, vol. 38, no. 11, pp. 2604–2620, 2020.

[6] L. You, J. Xiong, D. W. K. Ng, C. Yuen, W. Wang, and X. Gao, "Energy efficiency and spectral efficiency tradeoff in RIS-aided multiuser MIMO uplink transmission," *IEEE Transactions on Signal Processing*, vol. 69, pp. 1407–1421, 2020.

[7] X. Wei, D. Shen, and L. Dai, "Channel estimation for RIS assisted wireless communications—part ii: An improved solution based on double-structured sparsity," *IEEE Communications Letters*, vol. 25, no. 5, pp. 1403–1407, 2021.